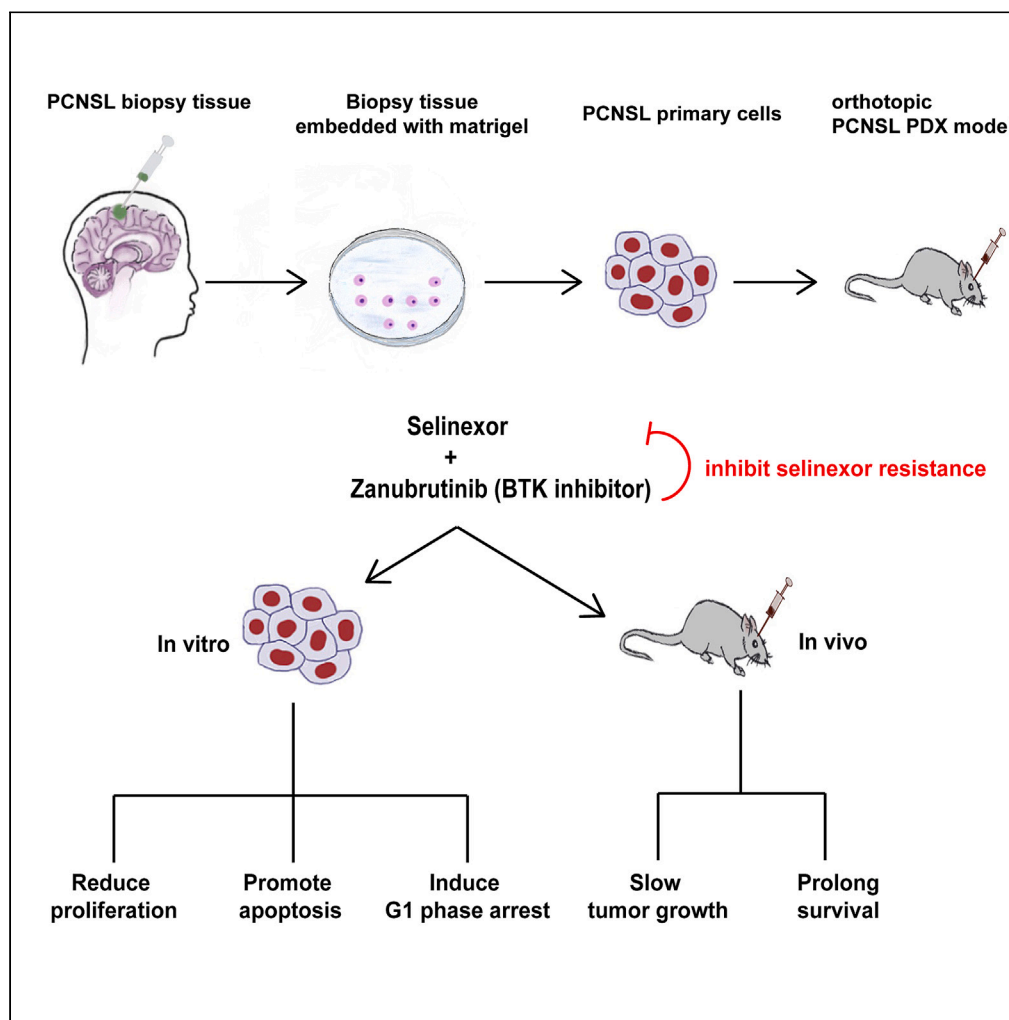


Article

Zanubrutinib delays selinexor resistance evolution in biopsy sample-derived primary central nervous system lymphoma models



Xiaohong Zheng,
Can Wang, Feng
Chen, ..., Chunlei
Han, Shuo Yin,
Wenbin Li

liwenbin@ccmu.edu.cn

Highlights

Establishment of PCNSL cells fills the gap of PCNSL cell line scarcity

The addition of zanubrutinib to selinexor has synergistic antitumor effect on PCNSL

Zanubrutinib prevents selinexor resistance in PCNSL by inhibiting AKT signaling

Zheng et al., iScience 27, 109799
May 17, 2024 © 2024 The Author(s). Published by Elsevier Inc.
<https://doi.org/10.1016/j.isci.2024.109799>



Article

Zanubrutinib delays selinexor resistance evolution in biopsy sample-derived primary central nervous system lymphoma models

Xiaohong Zheng,^{1,4} Can Wang,^{1,4} Feng Chen,¹ Shenglan Li,¹ Hua Zhang,² Gehong Dong,³ Shoubo Yang,¹ Xun Kang,¹ Zhuang Kang,¹ Chunlei Han,² Shuo Yin,¹ and Wenbin Li^{1,5,*}

SUMMARY

Primary central nervous system lymphoma (PCNSL) is a rare and aggressive lymphoma of the brain with poor prognosis. The scarcity of cell lines established using PCNSL makes it difficult to conduct preclinical studies on new drugs. We aimed to explore the effect of selinexor combined with zanubrutinib in PCNSL using established PCNSL cells and an orthotopic PCNSL model. Primary PCNSL cells were successfully cultured. Selinexor inhibited proliferation, induced G1 phase arrest, and promoted apoptosis, however, induced drug resistance in PCNSL. Selinexor combined with zanubrutinib had a synergistic effect on PCNSL and prevented the onset of selinexor resistance in PCNSL by inhibiting AKT signaling. Moreover, selinexor combined with zanubrutinib notably slowed tumor growth and prolonged survival compared to that of the control. Overall, the addition of zanubrutinib to selinexor monotherapy had a synergistic effect *in vitro* and prolonged survival *in vivo*.

INTRODUCTION

Primary central nervous system lymphoma (PCNSL) is a rare and aggressive extranodal non-Hodgkin lymphoma (NHL) with poor prognosis. Although first-line chemotherapy based on high-dose methotrexate has a high remission rate, up to 50% of patients relapse and 10–15% have primary refractory disease.¹ The optimal treatment approach has yet to be established. Therefore, new therapeutic drugs are urgently needed to develop optimal treatment strategies. The scarcity of cell lines established from PCNSL makes it difficult to conduct experimental studies on new drugs,^{2,3} which greatly limits the preclinical efficacy evaluation of new therapeutic drugs for PCNSL.

In June 2020, selinexor was approved by the FDA for the treatment of systemic relapsed/refractory diffuse large B-cell lymphoma (DLBCL) after positive results were obtained in a phase IIb trial.⁴ In a clinical case study, selinexor was reported to inhibit refractory DLBCL with central nervous system (CNS) involvement.⁵ Approximately 90% of PCNSL cases are DLBCL.⁶ Thus, selinexor is a promising therapeutic drug for the treatment of PCNSL. Selinexor, a blood-brain barrier-permeable small molecule,⁷ selectively inhibits nuclear export compounds that inhibit exportin 1 (XPO1/CRM1) activity. This leads to the nuclear accumulation of tumor suppressor proteins and cell cycle regulators, which translate into cell-cycle arrest and specific anticancer activity.^{8,9} Selinexor has been shown to exhibit significant anti-tumor activity in phase I clinical trials for the treatment of both hematological malignancies and solid tumors.^{10–13} However, tumor cells easily develop resistance to selinexor, hindering its clinical application.

Activation of AKT-forkhead box O3 survival signaling is a key mechanism in selinexor resistance.¹⁴ PCNSL is highly dependent on B cell receptor (BCR) signaling,¹⁵ which is crucial for the proliferation and survival of tumor cells in various B-cell malignancies.¹⁶ BCR signaling activates the AKT signaling pathways by Bruton's tyrosine kinase (BTK),^{16,17} which plays a crucial role in BCR signaling. As BCR signaling in PCNSL is activated, BTK inhibitors inhibit BCR signal transduction and abrogate downstream pathways including AKT, ERK, and NF- κ B.¹⁸ Thus, targeting BTK using BTK inhibitors may be effective in patients with acquired selinexor resistance.

BTK inhibitors include both first- and next-generation inhibitors. Zanubrutinib is a next-generation, highly potent, selective, and irreversible BTK inhibitor developed by BeiGene for the treatment of B-cell malignancies.¹⁹ Designed to maximize target occupancy and minimize off-target binding, zanubrutinib has potential pharmacodynamic and pharmacokinetic advantages over the first-generation BTK inhibitor ibrutinib, a second-line treatment for PCNSL, included in the National Comprehensive Cancer Network (NCCN) guidelines.^{20,21} Recently, pre-clinical studies²² and clinical trials²³ demonstrated the efficacy of zanubrutinib for the treatment of systemic DLBCL. Therefore, zanubrutinib

¹Department of Neuro-Oncology, Cancer Center, Beijing Tiantan Hospital, Capital Medical University, Beijing, China

²Department of Neurosurgery, Beijing Tiantan Hospital, Capital Medical University, Beijing, China

³Department of Pathology, Beijing Tiantan Hospital, Capital Medical University, Beijing, China

⁴These authors contributed equally

⁵Lead contact

*Correspondence: liwenbin@ccmu.edu.cn

<https://doi.org/10.1016/j.isci.2024.109799>



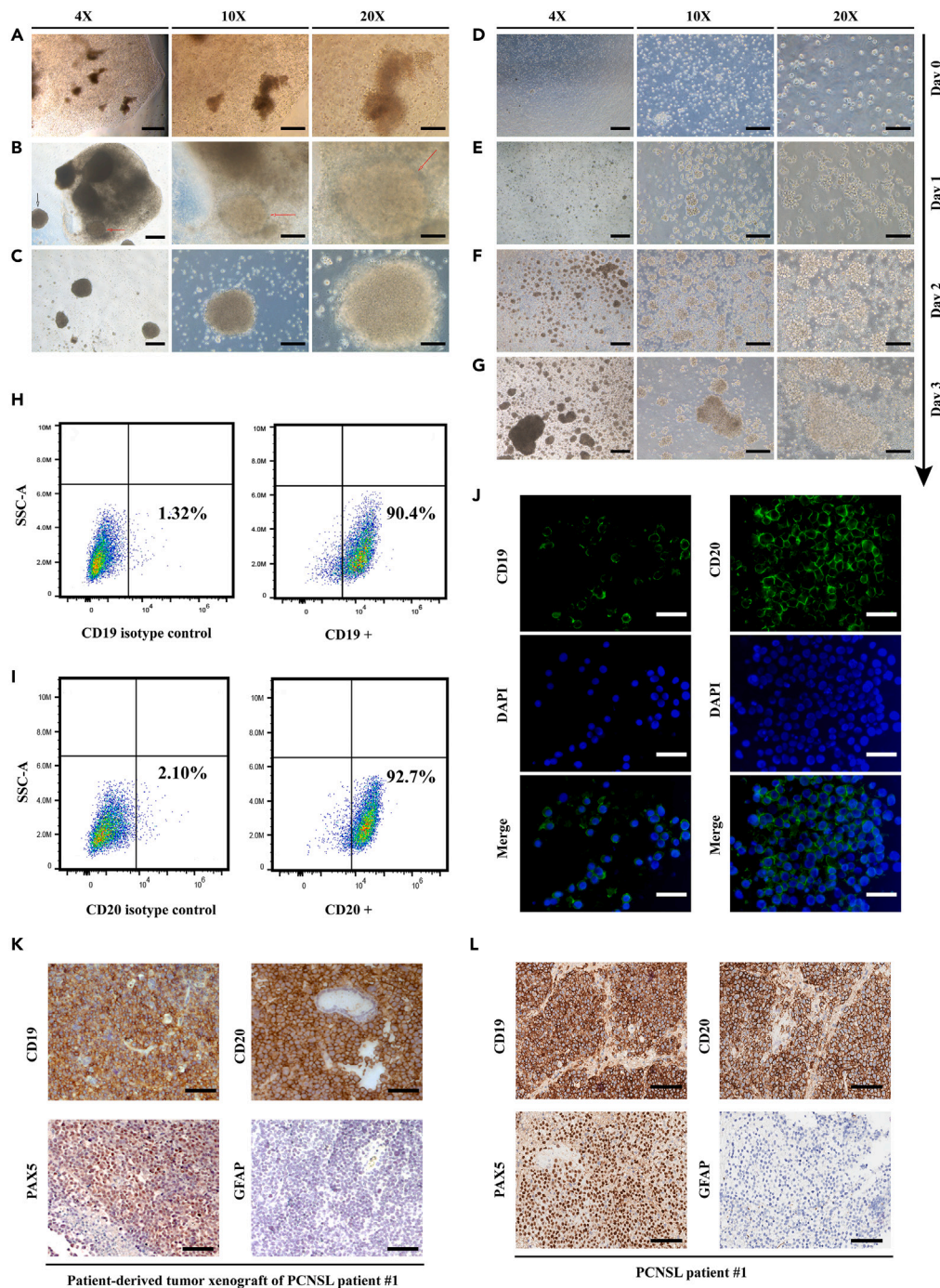


Figure 1. PCNSL primary cells established from the stereotaxic biopsy tissue of PCNSL patient #1

- (A) Biopsy tissue was cut up and embed in Matrigel.
 (B) Cell clusters appeared in (red arrow) and outside (black arrow) the pellets wrapped with Matrigel after 21 days of culture.
 (C) The microscopic morphology of cell aggregates appearing outside the pellets wrapped with Matrigel.
 (D–G) The cell morphology from day 0 to day 3 after passage.
 (H) Detection of CD19 expression in primary cells using flow cytometry.
 (I) The expression of CD20 in primary cells determined by flow cytometry.
 (J) Immunofluorescence of CD19 and CD20 in primary cells.

Figure 1. Continued

(K) Immunohistochemical staining of CD19, CD20, PAX5, GFAP in patient-derived tumor xenograft.

(L) Immunohistochemical staining of CD19, CD20, PAX5, GFAP in PCNSL patient #1. The images in (A–G) show 4× (scale bar = 400 μm), 10× (scale bar = 200 μm) and 20× (scale bar = 100 μm) magnification. In (J) images taken at 40× (scale bar = 50 μm). (K) scale bar = 50 μm; (L) scale bar = 100 μm. PCNSL, primary central nerve system lymphoma.

may show promising results in the treatment of PCNSL. In addition, zanubrutinib might prevent the onset of selinexor-resistant clones by inhibiting the activation of downstream BCR targets, such as AKT, and when combined with selinexor, produce synergistic activity in PCNSL.

In this study, we successfully established primary PCNSL cells from biopsy tissue of patient and constructed an orthotopic PCNSL mice model. We used these models to evaluate the efficacy of selinexor and zanubrutinib alone and in combination in the treatment of PCNSL and to explore the possible mechanism of the combination of selinexor and zanubrutinib in preventing the onset of selinexor-resistant clones.

RESULTS**Primary PCNSL cells established from the stereotaxic biopsy tissue of the patient**

According to the culture method of cerebral and glioma organoids,^{24,25} biopsy tissues from three patients (patients #1, #2, and #3) with PCNSL were dissected, embedded in Matrigel, and then cultured in special medium (Figures 1A, S2, and S3). In the biopsy tissue of patient #1, after 21 days of culture, microscopic observations revealed that cell clusters appeared inside and outside the pellets wrapped in Matrigel, and the cell clusters exhibited dense and spherical characteristics (Figures 1B and 1C). We passaged the cell clusters that appeared outside the pellets wrapped in Matrigel (Figure 1C). On day 0 after passage, the cells exhibited suspension characteristics and a round appearance with large nuclei (Figure 1D). With the extension of culture time, the cell density gradually increased and the cells aggregated into clusters (Figures 1E–1G). The cells exhibited suspended clusters, similar to those of most systemic DLBCL cell lines. When the density of cultured primary cells reached 90%, cell passage was started, and passage was performed every three days. Primary cells were frozen and thawed.

To verify whether the cultured cells were PCNSL, we first examined the expression of specific markers for the diagnosis of B-cell lymphoma²⁶ (CD19 and CD20) using flow cytometry and immunofluorescence. The flow cytometry results showed that the positivity rates of CD19 and CD20 were 90.4% and 92.7%, respectively (Figures 1H and 1I). The immunofluorescence results showed that CD19 and CD20 were highly expressed in the cell membranes (Figure 1J). These results provided preliminary evidence that the cultured cells were DLBCL. We then subcutaneously implanted cultured cells from patient #1 into NTG mice. After 12 days, the cultured cells formed patient-derived tumor xenograft (PDX) in mice. The incidence of tumors was approximately 95%. After 28 days, xenograft formation was eliminated by immunohistochemical staining (Figure S4). The staining results revealed the histological characteristics of DLBCL with positive expression of CD19, CD20, and PAX5 and negative expression of GFAP (Figure 1K), which was consistent with the histopathological results of patient #1 with PCNSL (Figure 1L). These data confirmed that the cells established from the stereotaxic biopsy tissue of the patient were PCNSL cells.

Primary cultured cells established from patients #2 and #3 and their validation are shown in Figures S2 and S3. Three primary cultured cells derived from three PCNSL patients had the same cell morphology and similar gene expression (Tables S1–S3) and we selected the primary cultured cells of patient #1 and patient #2 for subsequent experiments in this study.

Selinexor has anti-tumor effects and exhibits drug resistance on PCNSL

Based on the PCNSL cells established in this study, we performed a cell viability assay to examine the effects of selinexor on PCNSL. The half-maximal inhibitory concentrations (IC₅₀) of selinexor in PCNSL cells from patient #1 and PCNSL cells of patient #2 were 159 nM (Figure 2A) and 66 nM (Figure S5A), respectively. Time-course analysis of cell death revealed that prolonged exposure to selinexor had a greater inhibitory effect on PCNSL cell proliferation (Figures 2B and S5B). To further study the effect of selinexor on PCNSL, we performed whole-transcriptome analyses of PCNSL primary cells (from patient #1) treated with selinexor. KEGG analysis indicated that cell cycle, DNA replication, and apoptosis signaling pathways were significantly enriched (Figure 2C). Consistent with the KEGG results, the cell cycle analysis indicated that the percentage of PCNSL cells in the G1 phase increased from 58.9% in the control group to 79.1% in the selinexor-treated group (Figure 2D). Apoptosis analysis showed that the annexin V-positive population was enhanced in PCNSL cells treated with selinexor (Figure 2E). These results show that selinexor inhibited proliferation, induced G1 phase arrest, and promoted apoptosis in PCNSL cells, ultimately resulting in anti-tumor effects.

A previous study has reported that selinexor exhibit drug resistance in acute myeloid leukemia (AML) and activation of AKT survival signaling is a key mechanism for selinexor resistance.¹⁴ To determine whether selinexor resistance occurs in PCNSL, we first performed heatmap analysis of related target genes of AKT signaling pathway based on transcriptome results. The results indicated that the expression of AKT upstream pathway molecules (PIK3CA, PIK3AP1, PIK3CD, and PIK3C2A), AKT2, AKT1S1, and downstream pathway molecules (MYC) was upregulated in the selinexor treatment group (Figure 2F). Furthermore, western blotting results showed that PCNSL cells exhibited notable upregulation of p-AKT upon treatment with selinexor (Figure 2G). These results suggest that selinexor resistance is evolving in PCNSL.

Combination of selinexor and zanubrutinib have a synergistic effect on the induction of PCNSL cell death

To prevent the onset of selinexor-resistant clones in PCNSL, selinexor was combined with zanubrutinib (an inhibitor of BTK and AKT) to treat PCNSL. The IC₅₀ of zanubrutinib in PCNSL cells of patient #1 and PCNSL cells of patient #2 was 33.688 μM (Figure S6) and 20.95 μM

PCNSL cell from patient #1

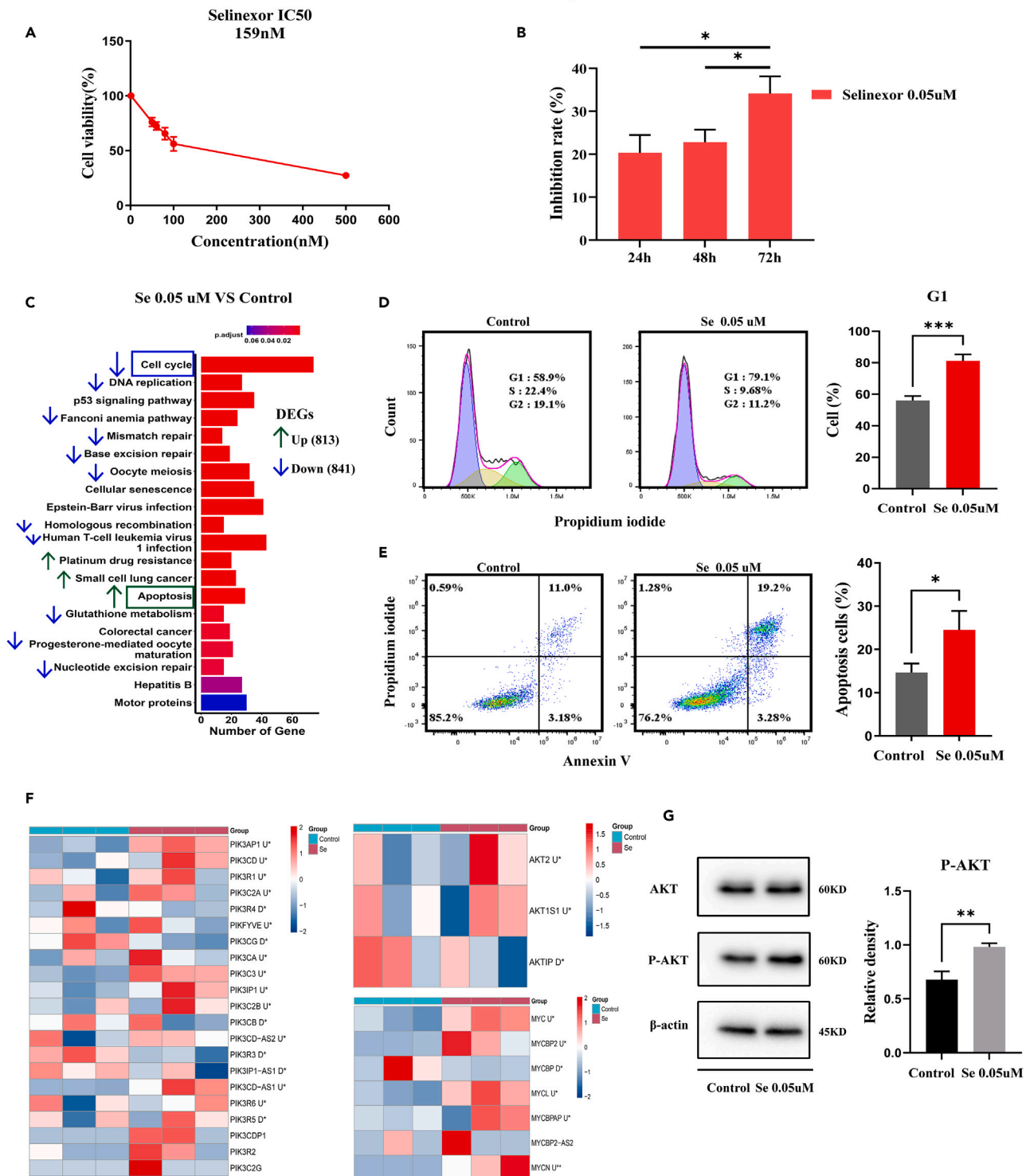


Figure 2. Selinexor has anti-tumor effects and exhibits drug resistance on PCNSL

The PCNSL cells used in the experiment established from patients #1.

(A) IC50 determination of selinexor in PCNSL cells.

(B) PCNSL cells were treated with selinexor for 24 h, 48 h and 72 h, cell viability was monitored by CCK8 assay.

Figure 2. Continued

(C) The top 20 enriched item of significantly differential genes between the selinexor group and the control group in the KEGG analysis. The upward (green) and downward (blue) arrows represent the items of upregulated and downregulated genes enrichment in selinexor group, respectively. DEGs, differentially expressed genes (813 up-regulated genes and 841 down-regulated genes).

(D) Flow cytometry analysis shows increased G1 arrest that was seen in PCNSL cells treated with selinexor for 24 h.

(E) Flow cytometry profile showing selinexor promoted apoptosis in PCNSL cells treated with selinexor for 24 h.

(F) The heatmap of AKT pathway related target genes in selinexor group and control group. U* and D* indicate that the gene is upregulated and downregulated, respectively, and statistically significant ($p < 0.05$) in the selinexor group. Three columns represent for three biological replicates in each group. The color coding is $\log_2(\text{gene expression} + 1)$.

(G) Western blotting was performed to detect the expression of AKT and p-AKT in PCNSL cells. Error bars represent mean \pm SD. * $p < 0.05$, ** $p < 0.01$, *** $p < 0.001$. Se, selinexor.

(Figure S5C), selinexor together with increasing concentrations of zanubrutinib substantially increased the inhibition rate of PCNSL cell growth, and prolonged exposure (24 h, 48 h, and 72 h) to the combination had a notable effect on the inhibition of cell proliferation (Figures 3A–3C). To confirm the synergistic effect of selinexor and zanubrutinib on PCNSL, CI values were calculated (Figure 3D). The combined therapy showed a strong synergistic inhibitory effect on the growth of PCNSL cells at all tested doses, with CI values ranging from 0.156 to 0.504 (CI values < 1 indicate synergistic effects). In addition, we performed the above experiments using another PCNSL cell line (from patient #2) and observed similar results (Figures S5D–S5G). Overall, the combination of selinexor and zanubrutinib demonstrated long-term synergistic effects on the induction of PCNSL cell death.

To further study the synergistic effect of selinexor combined with zanubrutinib on PCNSL at the gene level; we performed difference analysis, KEGG analysis, and target gene heatmap analysis based on the RNA sequencing results. We used DESeq2 software for differential analysis, and genes with $|\log_2 \text{fold change}| > \log_2(1.5)$ and adjusted $p < 0.05$ were defined as differential genes (Files S1, S2, and S3). A total of 1654, 676, and 1211 differentially expressed genes were present in the selinexor, zanubrutinib, and selinexor + zanubrutinib co-treatment groups, respectively (Figure S7). KEGG analysis revealed that, similar to the selinexor group (Figure 2C), the zanubrutinib and combination treatment groups were significantly enriched in the cell cycle, DNA replication, and apoptosis (Figures 3E and 3F). Heatmap analysis of related target genes of the AKT signaling pathway revealed that selinexor combined with zanubrutinib downregulated the expression of AKT upstream pathway molecules (PIK3CA, PIK3AP1, PIK3CD, and PIK3C2A), AKT2, AKT1S1, and downstream pathway molecules (MYC) (Figure 3G), suggesting that zanubrutinib potentially prevents the onset of selinexor-resistant clones in PCNSL.

Combination of selinexor and zanubrutinib induce G1 arrest and promote apoptosis in PCNSL cells

KEGG results identified cell cycle and apoptosis as signaling hubs for PCNSL cell growth. To further determine whether the inhibition of cell growth by treatment with selinexor and zanubrutinib was associated with the cell cycle and apoptosis, we first used flow cytometry to analyze the cell cycle profiles of the treated cells. In PCNSL cells of patient #1, the percentage of G1 phase increased from $62.67 \pm 5.45\%$ in the control group to $87.07 \pm 0.85\%$ and $89.23 \pm 1.07\%$ in the combination treatment groups (Figure 4A). A corresponding decrease in the number of cells in the S phase was also observed. Consistent with these results, the expression of Cyclin A2 (which plays an essential role in the G1/S transition) and Cyclin B1 (which is necessary for the progression of cells into and out of the M phase) substantially decreased in cells co-treated with selinexor and zanubrutinib; however, treatment with single agents mildly affected the expression of these proteins (Figures 4B and 4C). Similar results were observed for other PCNSL cell lines (Patient #2, Figures S8A–S8C). These data demonstrate that selinexor and zanubrutinib induce G1 phase arrest.

To assess the effects of selinexor and zanubrutinib on apoptosis, we analyzed the levels of apoptosis in PCNSL cells after 24 h exposure to the indicated concentrations of selinexor and/or zanubrutinib. The annexin V-positive population was enhanced in PCNSL cells treated with selinexor in combination with zanubrutinib. In addition, the proportion of apoptotic cells in the combination therapy group was higher than that in the single drug group (Figure 4D). Similar results were observed in other PCNSL cells (Figure S8D). Thus, co-treatment with selinexor and zanubrutinib synergistically promotes apoptosis. Consistent with the results of annexin V staining, the expression of proteins associated with apoptosis also changed in response to treatment of PCNSL cells (Figures 4E–4G). Treatment with selinexor or zanubrutinib slightly increased the expression of the active forms of poly-ADP ribose polymerase (PARP) and caspase-3 (Figures S8E and S8F), whereas co-treatment drastically enhanced these effects (Figures 4E, 4F, S8E, and S8F). Treatment with this combination also increased the expression of the pro-apoptotic protein Bax (Figure 4G). These results show that selinexor and zanubrutinib promote apoptosis by activating the caspase-dependent pathway in PCNSL cells, ultimately resulting in cytotoxicity.

Overall, selinexor and zanubrutinib suppressed cell proliferation by inducing both cell-cycle arrest and apoptosis, with the combination treatment being the most effective.

Combination of selinexor and zanubrutinib inhibit BCR signal transduction and abrogate activation of AKT signaling pathway

Selinexor resistance led to increased nuclear export of cargo proteins, including tumor suppressor proteins and cell cycle regulators, thereby activating the AKT signaling pathway (Figure 5A). However, selinexor combined with zanubrutinib inhibited BCR signal transduction and blocked downstream pathways that promote cell survival, including AKT and ERK. Heatmap analysis showed that the expression of AKT

PCNSL cell from patient #1

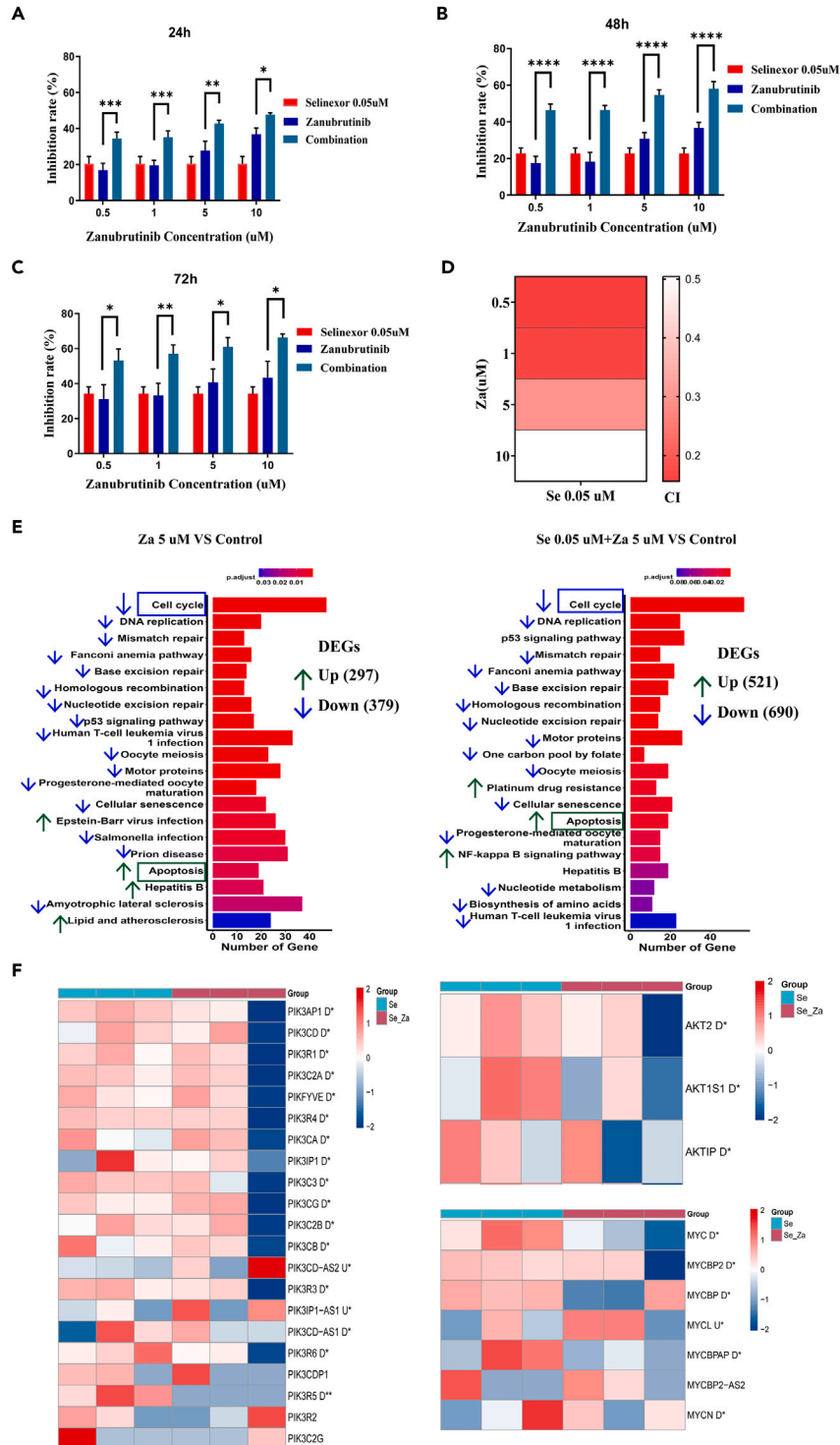


Figure 3. Selinexor and zanubrutinib have a synergistic effect on the induction of PCNSL cells death

The PCNSL cells used in the experiment established from patients #1.

(A–C) PCNSL cells were treated with fixed concentration of selinexor (0.05 μ M) and different concentrations of zanubrutinib for 24 h (A), 48 h (B) and 72 h (C), cell viability was monitored by CCK8 assay.

(D) Heatmap of combination index (CI) for each combination of selinexor and zanubrutinib. CI values <1 indicates synergism effects.

Figure 3. Continued

(E) The top 20 enriched item of significantly differential genes between the treatment group and the control group in the KEGG analysis. The upward (green) and downward (blue) arrows represent the upregulated and downregulated items in treatment group, respectively. DEGs, differentially expressed genes.

(F) The heatmap of AKT pathway related target genes in the combination of selinexor and zanubrutinib group and selinexor group. U* and D* indicate that the gene is upregulated and downregulated, respectively, and statistically significant ($p < 0.05$) in the combination group. Three columns represent for three biological replicates in each group. The color coding is $\log_2(\text{gene expression} + 1)$. Error bars represent mean \pm SD. * $p < 0.05$, ** $p < 0.01$, *** $p < 0.001$, **** $p < 0.0001$. PCNSL, primary central nerve system lymphoma; Se, selinexor; Za, zanubrutinib; Se_Za, selinexor 0.05 μM combined with zanubrutinib 5 μM .

signaling pathway-related target genes was upregulated in the selinexor group (Figure 2G), whereas these genes were downregulated in the selinexor + zanubrutinib group (Figure 3G), suggesting that the combination of selinexor and zanubrutinib could prevent selinexor resistance. Although there was no statistically significant difference in the upregulation of *p*-AKT and *p*-BTK in selinexor treated PCNSL cells (from patient #1) compared to the control group (Figure 5B), there was a significant difference in the upregulation of *p*-AKT and *p*-BTK in PCNSL cells from patient #2 (Figures S9A and S9B). What's more, the expression of *p*-AKT, *p*-BTK, and *p*-ERK substantially decreased in PCNSL cells co-treated with selinexor and zanubrutinib (Figures 5B, 5C, and S9). To further determine the mechanism by which selinexor combined with zanubrutinib prevents the onset of selinexor resistance in PCNSL, an AKT activator and inhibitor were added for cell proliferation and western blot analyses. The rate of PCNSL cell inhibition was reduced in the selinexor, zanubrutinib, and combination groups after the addition of the AKT activator, whereas the rate of inhibition increased after the addition of the AKT inhibitor (Figure 5D). Consistent with the results of cell proliferation analysis, the expression of *p*-AKT was decreased in PCNSL cells after the addition of the AKT inhibitor (Figure 5E). Moreover, the ERK inhibitor was added for cell proliferation assay to rule out ERK signaling. The rate of PCNSL cell inhibition did not increase after the addition of the ERK inhibitor (Figure S10). These results suggest that selinexor induces drug resistance, and co-administration of selinexor and zanubrutinib can prevent the onset of selinexor resistance in PCNSL by inhibiting BCR signal transduction and abrogating the activation of the AKT signaling pathway.

Selinexor and zanubrutinib have anti-tumor effect in orthotopic PCNSL PDX models

We assessed the effect of selinexor alone and in combination with zanubrutinib on tumor growth in an orthotopic PCNSL PDX model (Figure 6A). Bioluminescent PCNSL cells were injected into the murine cerebrum to generate orthotopic xenografts. Initial radiance signals showed similar tumor sizes in the four groups, whereas tumor growth continued to slow in the treated mice (Figures 6B and 6C). Compared to that of the control, tumor growth was robustly slower in mice treated with the combination treatment. In survival analysis, the treated mice survived markedly longer than the control mice (median survival for mice treated with selinexor: 35.5 days vs. median survival of control mice: 26 days, $p = 0.037$; zanubrutinib, 39 days vs. control, $p = 0.042$; selinexor combined with zanubrutinib, 40 days vs. control, $p = 0.008$; Figure 6D). The combination treatment increased the survival of mice compared with selinexor, whereas no significant difference was observed between the combination and zanubrutinib (combination vs. selinexor, $p = 0.037$; combination vs. zanubrutinib, $p = 0.307$).

To evaluate tumor proliferation and apoptosis after different treatments, Ki-67 and TUNEL were investigated and quantified in paraffin sections of brain samples collected from PCNSL xenografts. Compared to tumors treated with zanubrutinib monotherapy, those treated with combination therapy exhibited reduced Ki-67 expression (Figures 6E and 6F). Furthermore, consistent with the *in vitro* data, co-treatment with selinexor and zanubrutinib substantially increased apoptosis compared with treatment with each agent alone (Figure 6G). Collectively, these results demonstrated that selinexor and zanubrutinib synergistically suppressed tumor growth and increased tumor cell apoptosis *in vivo*, confirming our *in vitro* findings.

DISCUSSION

Cell lines and animal models of PCNSL are required to dissect their molecular pathogenesis and evaluate novel therapeutics. Although ISAO et al. established a B-cell lymphoma cell line from a patient with primary CNS lymphoma in 1978,²⁷ we had previously attempted the construction and cultivation methods and failed. The low success rate of this protocol may be one of the reasons for the scarcity of primary PCNSL cells and cell lines until now. HKBML (Riken, Japan), another PCNSL cell line, was established by Ishiwata et al. in 1991. In recent years, there have been a few PCNSL studies based on this cell line in Japan. Unfortunately, the detailed protocol for the establishment of HKBML is not available. Furthermore, due to the scarcity of PCNSL cells, it is the most commonly used method to establish PCNSL animal model by intracranial injection of human systemic lymphoma cell lines such as Raji,^{28,29} MC116 B,^{30–32} and murine lymphoma cell lines such as A20.IIA^{33,34} and BAL17.³⁵ However, as these lymphoma cell lines are not established from PCNSL, the intracranial models constructed from these cells are brain metastasis models for lymphoma rather than PCNSL models. Recently, a PCNSL orthotopic PDX model established from biopsy samples of patients with PCNSL has become an accurate PCNSL model.^{36,37} However, PCNSL PDX models have a long passage cycle and individual variability, which notably limits the exploration of the molecular mechanisms underlying PCNSL at a deep level. Therefore, PCNSL cells must be established, and the construction method must be repeated to facilitate orthotopic animal model construction and drug development for PCNSL.

The unique tumor microenvironment of PCNSL may explain the reason for scarcity of PCNSL cell lines and the difficulty establish. Currently, there is no recognized cell culture system or method for treating PCNSL. Conventional culture systems for systemic DLBCL cell lines may not be suitable for the stable growth and passage of PCNSL cells. We referred numerous related literature for overcoming

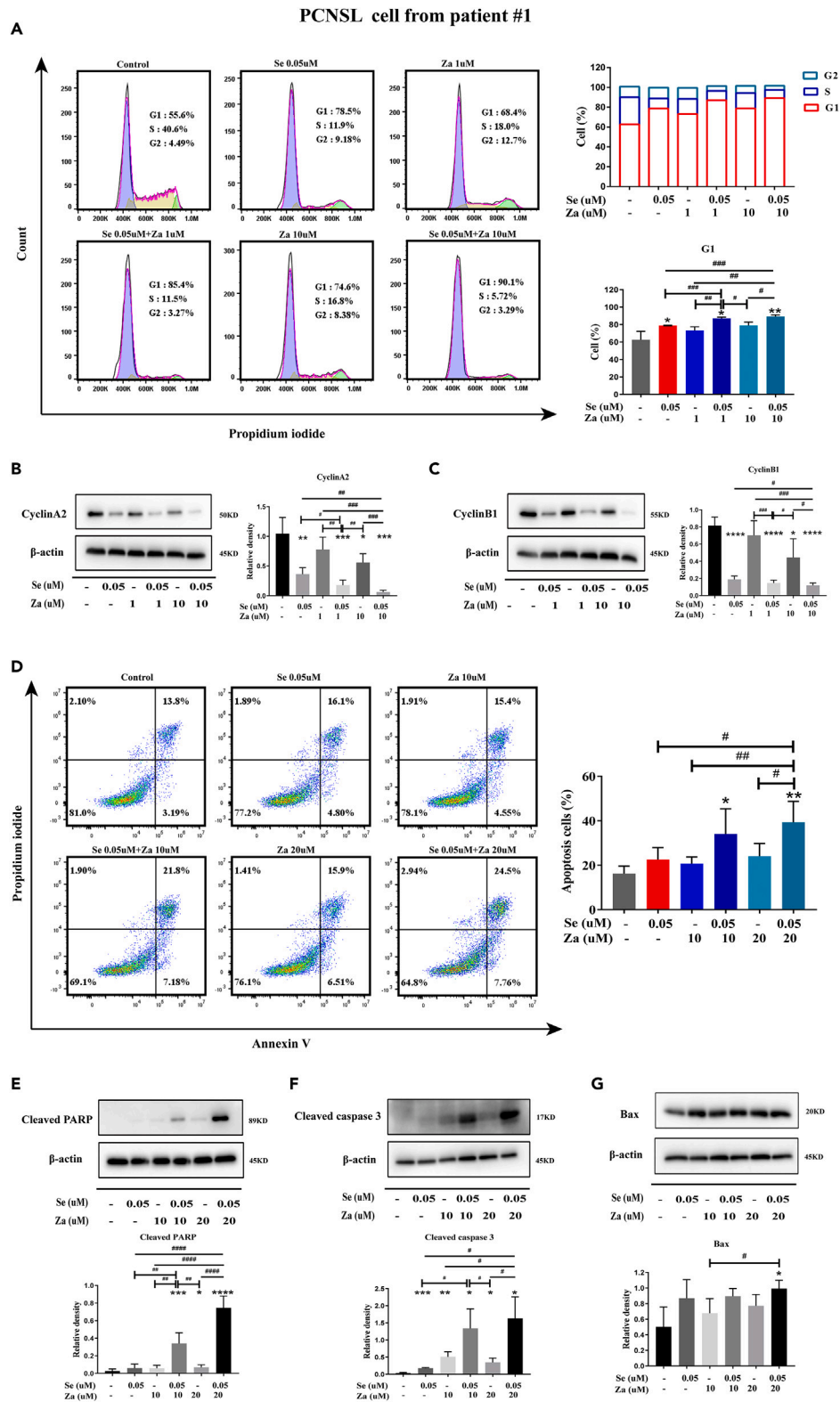


Figure 4. Selinexor and zanubrutinib induce G1 arrest and promoted apoptosis in PCNSL cells established from patients #1

(A) Flow cytometry analysis shows increased G1 arrest that was seen in PCNSL cells treated with different concentrations of zanubrutinib in the presence or absence of fixed concentration of selinexor for 24 h. Representative pictures are shown.

Figure 4. Continued

(B and C), The protein levels of cell cycle related proteins cyclin A2 and cyclin B1 in PCNSL cells treated with fixed concentration of selinexor and different concentrations of zanubrutinib.

(D) Flow cytometry profile showing selinexor and zanubrutinib alone or in combination promoted apoptosis in PCNSL cells. Representative pictures are shown.

(E–G) Western blotting was performed to detect the expression of cleaved PARP (E), cleaved caspase 3 (F) and bax (G) in PCNSL cells. Error bars represent mean \pm SD. * $p < 0.05$, ** $p < 0.01$, *** $p < 0.001$, **** $p < 0.0001$, each treatment group compared with control group; # $p < 0.05$, ## $p < 0.01$, ### $p < 0.001$, #### $p < 0.0001$, combination group compared with single-drug group. PCNSL, primary central nerve system lymphoma. Se, selinexor. Za, zanubrutinib.

these issues. Finally, referring to the cultivation methods for cerebral and glioma organoids,^{24,25} we dissected limited biopsy tissues from patients with PCNSL into pieces, embedded them in Matrigel, and cultured them in a specific homemade medium. This culture medium simulates the CNS environment necessary for the survival of PCNSL. We successfully established primary cells from biopsy tissues with a success rate of 100% (three PCNSL cells were successfully established from three patients with PCNSL). The successful construction of PCNSL cells not only fills the gap in scarcity PCNSL cell lines, but also facilitates the preclinical evaluation of new drugs and in-depth research on PCNSL biology.

PCNSL has advanced significantly in treatment and has improved survival; however, relapse is common, and long-term survival remains poor. Additionally, an optimal standard treatment for PCNSL is yet to be established. Therefore, new drugs must be developed for the treatment of PCNSL. Selinexor is a relatively well-studied anti-tumor agent. Preclinical activity for selinexor have been documented against T cell acute lymphoblastic leukemia,³⁸ AML,³⁸ multiple myeloma,³⁹ chronic lymphocytic leukemia (CLL),⁴⁰ NHL,⁴¹ and solid tumors.⁸ Phase IIb studies of selinexor have shown that it is well tolerated in patients with DLBCL, with an overall response rate of 28% (36/127), which has led to its FDA approval for the treatment of relapsed/refractory DLBCL. The efficacy of selinexor against DLBCL makes it a promising candidate for the treatment of PCNSL. However, selinexor can also exhibit drug resistance. Emdal et al.¹⁴ profiled selinexor signaling responses using phosphoproteomics in samples and cell lines of patients with primary AML and found that activated AKT survival signaling is a key selinexor resistance mechanism. Our heatmap analysis indicated that the expression of target genes related to the AKT signaling pathway was upregulated in selinexor-treated PCNSL cells. Consistent with the results of the heatmap analysis, western blotting showed increased *p*-AKT expression in PCNSL cells after treatment with selinexor. Moreover, after adding the AKT inhibitor to the selinexor group, the inhibition rate of PCNSL cells increased, and the expression of *p*-AKT decreased. These results suggest that selinexor treatment may initiate resistance in PCNSL cells. Thus, it is crucial to discover another drug that can overcome activated AKT signaling and that has synergistic effects when combined with selinexor.

The PI3K/AKT and ERK pathways are mainly regulated by BCR signaling in DLBCL and BCR is essential for the proliferation and survival of malignant B cells.⁴² Owing to the significant role of BTK in proximal BCR signaling, the inhibitor is considered to primarily target BCR signaling. BTK inhibitors are small molecules with a promising CNS distribution that bind to BTK, inhibit BCR signal transduction, and block downstream pathways, including AKT and ERK. Ibrutinib, a first-generation BTK inhibitor, has been widely used in hematological malignancies and is recommended by the NCCN guidelines for the second-line treatment of PCNSL. However, ibrutinib is prone to off-target effects and adverse events such as bleeding, rash, and diarrhea.⁴³ Zanubrutinib is a new and next-generation selective BTK inhibitor that has been reported to have greater specificity for BTK and a lower proportion of off-target effects compared with ibrutinib.^{20,21} Preclinical studies have shown the efficacy of zanubrutinib in the treatment of B-cell malignancies.^{22,44} In the present study, we observed decreased expression of *p*-BTK, *p*-AKT, and *p*-ERK in the zanubrutinib-treated PCNSL group, indicating that zanubrutinib inhibited BTK activation, thereby blocking oncogenic signals downstream of BCR. Compared to monotherapy with zanubrutinib, the combination of selinexor and zanubrutinib resulted in decreased expression of *p*-BTK, *p*-AKT, and *p*-ERK. At the gene level, this combination downregulated the expression of genes related to the AKT pathway. Moreover, the elevated inhibition of PCNSL cells and reduced expression of *p*-AKT were more pronounced with the addition of the AKT inhibitor in the combination group. These data suggest that the combination of selinexor and zanubrutinib prevents the development of selinexor resistance.

A previous study indicated increased survival in mouse OCI-LY10 CNS lymphoma and PCNSL PDX models after treatment with selinexor and the first-generation BTK inhibitor ibrutinib.⁹ However, no preclinical and clinical studies have been conducted on the treatment of PCNSL with selinexor combined with zanubrutinib. In the present study, based on the PCNSL cells that we have established, we investigated whether the combination of selinexor and novel BTK inhibitor zanubrutinib had synergistic anti-tumor effects in PCNSL. Our findings revealed the synergistic effects of these two agents on the reduction in proliferation, promotion of apoptosis, induction of G1 phase arrest, and downregulation of BCR and downstream signaling in PCNSL cells. In addition, we established an orthotopic PCNSL PDX model to evaluate the efficacy and survival of selinexor and zanubrutinib in the treatment of PCNSL. We observed that selinexor combined with zanubrutinib robustly slowed tumor growth and prolonged survival compared to the control group. Overall, the combination of selinexor and zanubrutinib had a synergistic anti-tumor effect *in vitro* and prolonged survival *in vivo*.

In summary, cell lines for PCNSL remain scarce. We developed a reliable protocol for establishing PCNSL primary cultures, cell lines, and an orthotopic PCNSL model based on biopsy tissues. Based on the PCNSL cells that we established and the orthotopic PCNSL PDX model, we evaluated the effects of the combination of selinexor and zanubrutinib on PCNSL and demonstrated that co-treatment had a synergistic effect *in vitro* and increased survival *in vivo*. Furthermore, we observed that this combination prevented the onset of selinexor resistance in PCNSL by inhibiting BCR signal transduction and abrogating the activation of the AKT signaling pathway. The successful establishment of PCNSL cells from biopsies fills the gap in the scarcity PCNSL cell lines and provides a solid foundation for evaluating new therapeutic methods for PCNSL. Our preclinical study paves the way for testing selinexor in combination with zanubrutinib for the treatment of PCNSL and provides a rational basis for future clinical investigations.

PCNSL cell from patient #1

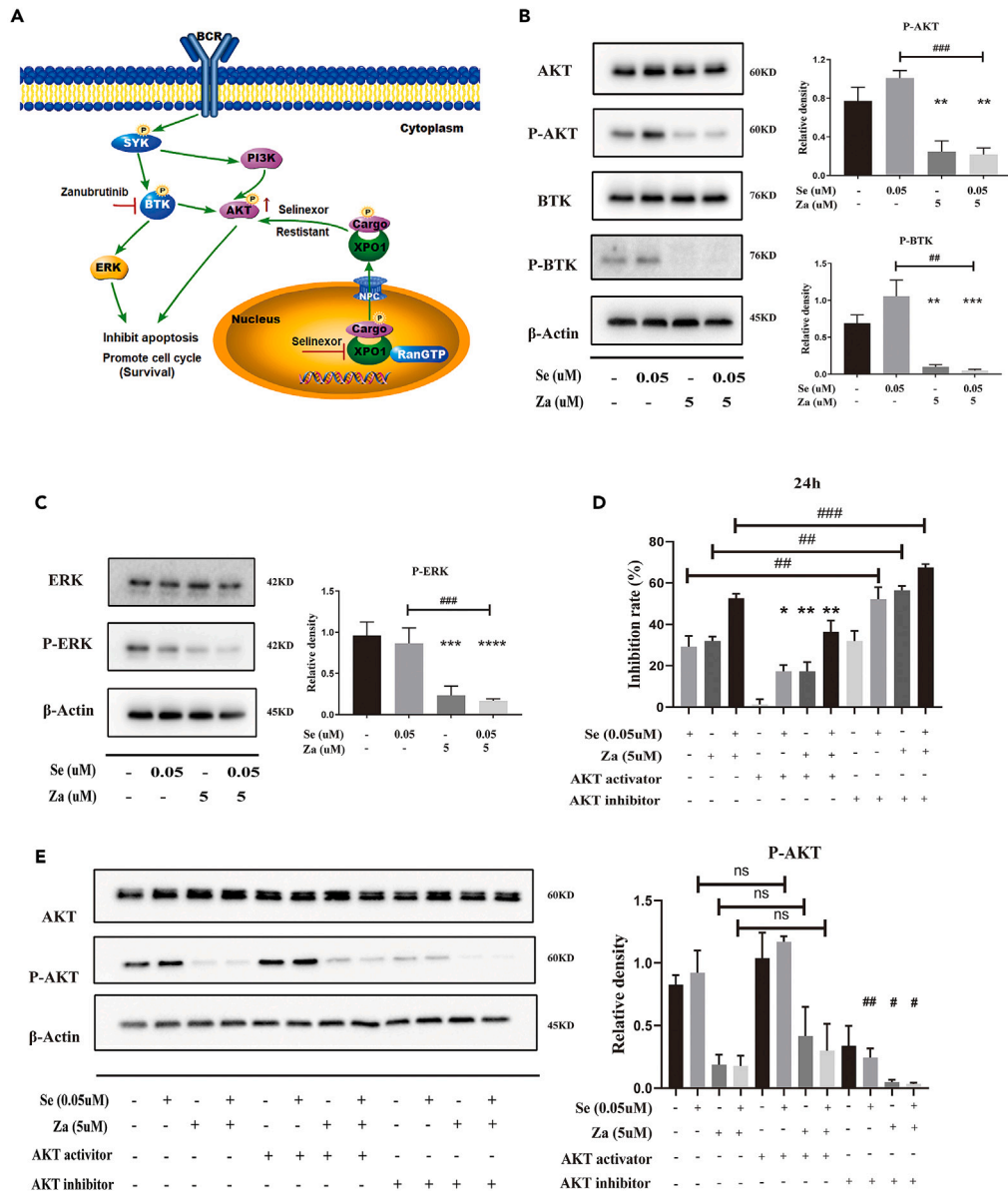


Figure 5. The combination of selinexor and zanubrutinib inhibit BCR signal transduction and abrogate activation of AKT signaling pathway

The PCNSL cells used in the experiment established from patients #1.

(A) Selinexor resistance leads to increased nuclear export of cargo proteins, thereby activating the AKT signaling pathway (red arrow). Zanubrutinib inhibit BTK and abrogate downstream pathways that promote cell survival, such as AKT and ERK.

(B) Representative western blotting result demonstrates that the expressions of p-AKT and p-BTK were up-regulated in the PCNSL cells treated with selinexor alone, while significantly decreased in the PCNSL cells treated with selinexor and zanubrutinib.

(C) Representative western blotting result shows the expression of p-ERK not only decreased in PCNSL cells treated with selinexor and zanubrutinib alone but also significantly decreased in PCNSL cells treated with the combination of selinexor and zanubrutinib.

(D) Cell proliferation analysis of PCNSL cells treated with selinexor 0.05 μ M, zanubrutinib 5uM, AKT activator (SC79 1uM) and AKT inhibitor (MK-2206 0.5uM) alone or in combination for 24 h.

(E) Representative western blotting result of PCNSL cells treated with selinexor 0.05 μ M, zanubrutinib 5uM, AKT activator (SC79 1uM) and AKT inhibitor (MK-2206 0.5uM) alone or in combination for 24 h. Error bars represent mean \pm SD. In (B) and (C), $^{*}p < 0.01$, $^{***}p < 0.001$, $^{****}p < 0.0001$, each treatment group compared with control group; $^{\#}p < 0.05$, $^{\#\#}p < 0.01$, $^{\#\#\#}p < 0.001$, combination group compared with single-drug group. In (D) and (E), $^{*}p < 0.05$, $^{**}p < 0.01$, $^{***}p < 0.001$, $^{****}p < 0.0001$, Se + AKT activator, Za + AKT activator and Se + Za + AKT activator compared with Se, Za and Se + Za, respectively; ns represents no statistical difference; $^{\#}p < 0.05$, $^{\#\#}p < 0.01$, $^{\#\#\#}p < 0.001$, Se + AKT inhibitor, Za + AKT inhibitor and Se + Za + AKT inhibitor compared with Se, Za and Se + Za, respectively. Se, selinexor; Za, zanubrutinib.

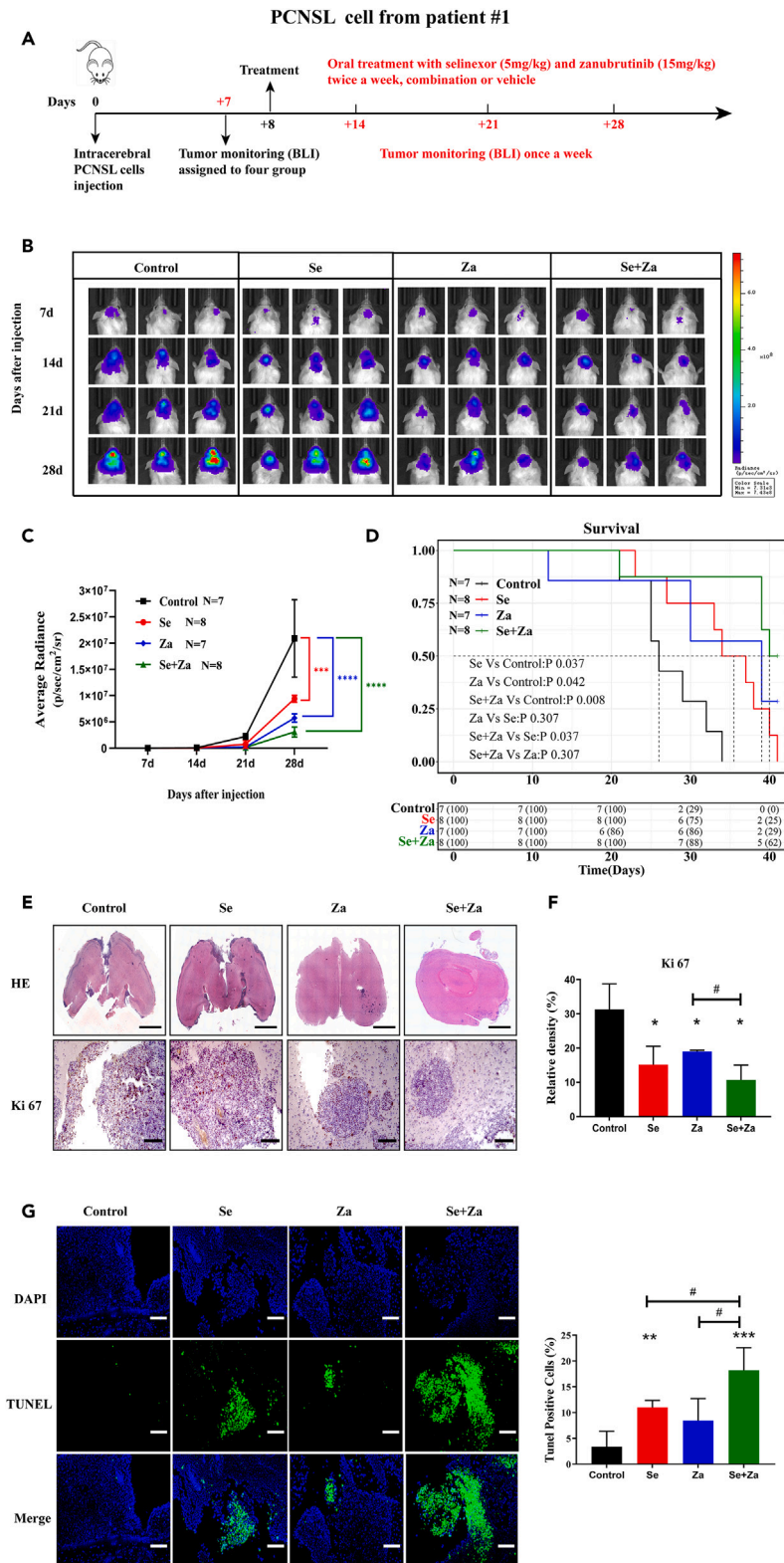


Figure 6. Selinexor and zanubrutinib have antitumor effects in orthotopic PCNSL models *in vivo*

The PCNSL cells used in the experiment established from patients #1.

(A) Scheme representing orthotopic PCNSL PDX model treatment and monitoring.

Figure 6. Continued

(B) Representative images of bioluminescence imaging of the PCNSL tumors.

(C) Tumor size as measured by bioluminescence imaging.

(D) Kaplan–Meier survival curve of mice in the four treatment groups.

(E) Representative pictures of H&E (Scale bar = 1.5 mm) and Ki 67 staining (Scale bar = 200 μ m) in sections are shown.

(F) The data represents the density of Ki 67 positivity cells for each section.

(G) Apoptosis of tumor tissue was assessed by the TUNEL assay. Representative images show apoptotic/fragmented DNA (green staining) and the corresponding cell nuclei (blue) staining. Scale bar = 100 μ m. Error bars represent mean \pm SD. * p < 0.05, ** p < 0.01, *** p < 0.001, **** p < 0.0001, each treatment group compared with control group; Se, selinexor; Za, zanubrutinib; Se+Za, selinexor combined with zanubrutinib.

Limitations of the study

A limitation of this analysis is that no significant difference was observed between the combination treatment and zanubrutinib treatment alone (p = 0.307) in the survival analysis. Possible reasons for this are as follows: First, this may be related to the fact that the sample size was not large enough (N = 7 or N = 8). The two survival curves for combination therapy and zanubrutinib did not intersect, and a statistical difference may have been there, as the sample size increased. Second, the mice were not treated with zanubrutinib for a sufficient time (twice a week for three weeks), resulting in insignificant differences between the two groups.

STAR★METHODS

Detailed methods are provided in the online version of this paper and include the following:

- **KEY RESOURCES TABLE**
- **RESOURCE AVAILABILITY**
 - Lead contact
 - Materials availability
 - Data and code availability
- **EXPERIMENTAL MODEL AND STUDY PARTICIPANT DETAILS**
 - Primary cells
 - Animal
- **METHOD DETAILS**
 - Establishment of PCNSL primary cells
 - Drugs and reagents
 - Flow cytometry
 - Immunofluorescence
 - Cell proliferation assay
 - Apoptotic analysis, cell-cycle assays, and TUNEL assay
 - RNA sequencing and analysis
 - Western blotting
 - Hematoxylin-eosin (HE) and immunohistochemical (IHC) staining
 - Subcutaneous and orthotopic PCNSL xenograft mice models
- **QUANTIFICATION AND STATISTICAL ANALYSIS**
 - Statistical analysis

SUPPLEMENTAL INFORMATION

Supplemental information can be found online at <https://doi.org/10.1016/j.isci.2024.109799>.

ACKNOWLEDGMENTS

This work was supported by grants from Clinical Major Specialty Projects of Beijing, and Talent Introduction Foundation of Tiantan Hospital (RCYJ-2020-2025-LWB). We thank BeiGene Co., Ltd. (Beijing, China) for the kind gifts of the zanubrutinib.

AUTHOR CONTRIBUTIONS

X.H.Z., C.W. and W.B.L. designed the study and prepared the manuscript. X.H.Z. produced the main draft of the text and the figures. X.H.Z., C.W., L.S.L., S.B.Y., X.K., Z.K. and S.Y. performed the experiments. H.Z. and C.L.H. provided tumor specimens. G.H.D. provided pathological pictures of patients. F.C. and W.B.L. reviewed manuscript.

DECLARATION OF INTERESTS

The authors declare no competing interests.

Received: December 4, 2023

Revised: March 18, 2024

Accepted: April 18, 2024

Published: April 23, 2024

REFERENCES

- Jahnke, K., Thiel, E., Martus, P., Herrlinger, U., Weller, M., Fischer, L., and Korfel, A.; German Primary Central Nervous System Lymphoma Study Group (2006). Relapse of primary central nervous system lymphoma: clinical features, outcome and prognostic factors. *J. Neuro Oncol.* 80, 159–165. <https://doi.org/10.1007/s11060-006-9165-6>.
- Deckert, M., Montesinos-Rongen, M., Brunn, A., and Siebert, R. (2014). Systems biology of primary CNS lymphoma: from genetic aberrations to modeling in mice. *Acta Neuropathol.* 127, 175–188. <https://doi.org/10.1007/s00401-013-1202-x>.
- You, H., Wei, L., and Kaminska, B. (2021). Emerging insights into origin and pathobiology of primary central nervous system lymphoma. *Cancer Lett.* 509, 121–129. <https://doi.org/10.1016/j.canlet.2021.02.025>.
- Kalakonda, N., Maerevoet, M., Cavallo, F., Follows, G., Goy, A., Vermaat, J.S.P., Casasnovas, O., Hamad, N., Zijlstra, J.M., Bakhshi, S., et al. (2020). Selinexor in patients with relapsed or refractory diffuse large B-cell lymphoma (SADAL): a single-arm, multinational, multicentre, open-label, phase 2 trial. *Lancet. Haematol.* 7, e511–e522. [https://doi.org/10.1016/s2352-3026\(20\)30120-4](https://doi.org/10.1016/s2352-3026(20)30120-4).
- Bobillo, S., Abrisqueta, P., Carpio, C., Raheja, P., Castellví, J., Crespo, M., and Bosch, F. (2018). Promising activity of selinexor in the treatment of a patient with refractory diffuse large B-cell lymphoma and central nervous system involvement. *Haematologica* 103, e92–e93. <https://doi.org/10.3324/haematol.2017.181636>.
- Grommes, C., Rubenstein, J.L., DeAngelis, L.M., Ferreri, A.J.M., and Batchelor, T.T. (2019). Comprehensive approach to diagnosis and treatment of newly diagnosed primary CNS lymphoma. *Neuro Oncol.* 21, 296–305. <https://doi.org/10.1093/neuonc/nyy192>.
- Etchin, J., Berezovskaya, A., Conway, A.S., Galinsky, I.A., Stone, R.M., Baloglu, E., Senapedis, W., Landesman, Y., Kauffman, M., Shacham, S., et al. (2017). KPT-8602, a second-generation inhibitor of XPO1-mediated nuclear export, is well tolerated and highly active against AML blasts and leukemia-initiating cells. *Leukemia* 31, 143–150. <https://doi.org/10.1038/leu.2016.145>.
- Senapedis, W.T., Baloglu, E., and Landesman, Y. (2014). Clinical translation of nuclear export inhibitors in cancer. *Semin. Cancer Biol.* 27, 74–86. <https://doi.org/10.1016/j.semcancer.2014.04.005>.
- Jiménez, I., Carabía, J., Bobillo, S., Palacio, C., Abrisqueta, P., Pagès, C., Nieto, J.C., Castellví, J., Martínez-Ricarte, F., Escoda, L., et al. (2020). Repolarization of tumor infiltrating macrophages and increased survival in mouse primary CNS lymphomas after XPO1 and BTK inhibition. *J. Neuro Oncol.* 149, 13–25. <https://doi.org/10.1007/s11060-020-03580-y>.
- Savona, M., Garzon, R., Brown, P.d.N., Yee, K., Lancet, J.E., Gutierrez, M., Gabrail, N., Mau-Sorensen, M., Baz, R., Byrd, J.C., et al. (2013). Phase I Trial of Selinexor (KPT-330), A First-In-Class Oral Selective Inhibitor Of Nuclear Export (SINE) In Patients (pts) With Advanced Acute Myelogenous Leukemia (AML). *Blood* 122, 1440. <https://doi.org/10.1182/blood.V122.21.1440.1440>.
- Kuruwilla, J., Gutierrez, M., Shah, B.D., Gabrail, N.Y., de Nully Brown, P., Stone, R.M., Garzon, R., Savona, M., Siegel, D.S., Baz, R., et al. (2013). Preliminary Evidence Of Anti Tumor Activity Of Selinexor (KPT-330) In a Phase I Trial Of a First-In-Class Oral Selective Inhibitor Of Nuclear Export (SINE) In Patients (pts) With Relapsed/Refractory Non Hodgkin's Lymphoma (NHL) and Chronic Lymphocytic Leukemia (CLL). *Blood* 122, 90. <https://doi.org/10.1182/blood.V122.21.90.90>.
- Chen, C.I., Gutierrez, M., de Nully Brown, P., Gabrail, N., Baz, R., Reece, D.E., Savona, M., Trudel, S., Siegel, D.S., Mau-Sorensen, M., et al. (2013). Anti Tumor Activity Of Selinexor (KPT-330), A First-In-Class Oral Selective Inhibitor Of Nuclear Export (SINE) XPO1/CRM1 Antagonist In Patients (pts) With Relapsed/Refractory Multiple Myeloma (MM) Or Waldenstrom's Macroglobulinemia (WM). *Blood* 122, 1942. <https://doi.org/10.1182/blood.V122.21.1942.1942>.
- Gounder, M.M., Zer, A., Tap, W.D., Salah, S., Dickson, M.A., Gupta, A.A., Keohan, M.L., Loong, H.H., D'Angelo, S.P., Baker, S., et al. (2016). Phase IB Study of Selinexor, a First-in-Class Inhibitor of Nuclear Export, in Patients With Advanced Refractory Bone or Soft Tissue Sarcoma. *J. Clin. Oncol.* 34, 3166–3174. <https://doi.org/10.1200/jco.2016.67.6346>.
- Erdal, K.B., Palacio-Escat, N., Wigerup, C., Eguchi, A., Nilsson, H., Bekker-Jensen, D.B., Rönstrand, L., Kazi, J.U., Puissant, A., Itzykson, R., et al. (2022). Phosphoproteomics of primary AML patient samples reveals rationale for AKT combination therapy and p53 context to overcome selinexor resistance. *Cell Rep.* 40, 111177. <https://doi.org/10.1016/j.celrep.2022.111177>.
- Löw, S., Han, C.H., and Batchelor, T.T. (2018). Primary central nervous system lymphoma. *Ther. Adv. Neurol. Disord.* 11, 1756286418793562. <https://doi.org/10.1177/1756286418793562>.
- Pal Singh, S., Dammeijer, F., and Hendriks, R.W. (2018). Role of Bruton's tyrosine kinase in B cells and malignancies. *Mol. Cancer* 17, 57. <https://doi.org/10.1186/s12943-018-0779-z>.
- Craxton, A., Jiang, A., Kurosaki, T., and Clark, E.A. (1999). Syk and Bruton's tyrosine kinase are required for B cell antigen receptor-mediated activation of the kinase Akt. *J. Biol. Chem.* 274, 30644–30650. <https://doi.org/10.1074/jbc.274.43.30644>.
- Herman, S.E.M., Gordon, A.L., Hertlein, E., Ramanunni, A., Zhang, X., Jaglowski, S., Flynn, J., Jones, J., Blum, K.A., Buggy, J.J., et al. (2011). Bruton tyrosine kinase represents a promising therapeutic target for treatment of chronic lymphocytic leukemia and is effectively targeted by PCI-32765. *Blood* 117, 6287–6296. <https://doi.org/10.1182/blood-2011-01-328484>.
- Tam, C.S., Trotman, J., Opat, S., Burger, J.A., Cull, G., Gottlieb, D., Harrup, R., Johnston, P.B., Marlton, P., Munoz, J., et al. (2019). Phase 1 study of the selective BTK inhibitor zanubrutinib in B-cell malignancies and safety and efficacy evaluation in CLL. *Blood* 134, 851–859. <https://doi.org/10.1182/blood.2019001160>.
- Guo, Y., Liu, Y., Hu, N., Yu, D., Zhou, C., Shi, G., Zhang, B., Wei, M., Liu, J., Luo, L., et al. (2019). Discovery of Zanubrutinib (BGB-3111), a Novel, Potent, and Selective Covalent Inhibitor of Bruton's Tyrosine Kinase. *J. Med. Chem.* 62, 7923–7940. <https://doi.org/10.1021/acs.jmedchem.9b00687>.
- Syed, Y.Y. (2020). Zanubrutinib: First Approval. *Drugs* 80, 91–97. <https://doi.org/10.1007/s40265-019-01252-4>.
- Setiawan, S.A., Liu, W.Z., Weng, P.W., Lee, C.H., Yadav, V.K., Hardianti, M.S., Yeh, C.T., and Chao, T.Y. (2023). Synergistic disruption of BTK and BCL-2 causes apoptosis while inducing ferroptosis in double-hit lymphoma. *Eur. J. Pharmacol.* 943, 175526. <https://doi.org/10.1016/j.ejphar.2023.175526>.
- Song, Y., Sun, M., Qi, J., Xu, W., Zhou, J., Li, D., Li, J., Qiu, L., Du, C., Guo, H., et al. (2022). A two-part, single-arm, multicentre, phase I study of zanubrutinib, a selective Bruton tyrosine kinase inhibitor, in Chinese patients with relapsed/refractory B-cell malignancies. *Br. J. Haematol.* 198, 62–72. <https://doi.org/10.1111/bjh.18162>.
- Lancaster, M.A., Renner, M., Martin, C.A., Wenzel, D., Bicknell, L.S., Hurles, M.E., Homfray, T., Penninger, J.M., Jackson, A.P., and Knoblich, J.A. (2013). Cerebral organoids model human brain development and microcephaly. *Nature* 501, 373–379. <https://doi.org/10.1038/nature12517>.
- Hubert, C.G., Rivera, M., Spangler, L.C., Wu, Q., Mack, S.C., Prager, B.C., Couce, M., McLendon, R.E., Sloan, A.E., and Rich, J.N. (2016). A Three-Dimensional Organoid Culture System Derived from Human Glioblastomas Recapitulates the Hypoxic Gradients and Cancer Stem Cell Heterogeneity of Tumors Found In Vivo. *Cancer Res.* 76, 2465–2477. <https://doi.org/10.1158/0008-5472.can-15-2402>.
- Scheuermann, R.H., and Racila, E. (1995). CD19 antigen in leukemia and lymphoma diagnosis and immunotherapy. *Leuk. Lymphoma* 18, 385–397. <https://doi.org/10.3109/10428199509059636>.
- Miyoshi, I., Kubonishi, I., Yoshimoto, S., Hikita, T., Dabasaki, H., Tanaka, T., Kimura, I., Tabuchi, K., and Nishimoto, A. (1982). Characteristics of a brain lymphoma cell line derived from primary intracranial lymphoma. *Cancer* 49, 456–459. [https://doi.org/10.1002/1097-0142\(19820201\)49:3<456::aid-cncr2820490311>3.0.co;2-k](https://doi.org/10.1002/1097-0142(19820201)49:3<456::aid-cncr2820490311>3.0.co;2-k).

28. Tsukahara, T., Ohmine, K., Yamamoto, C., Uchibori, R., Ido, H., Teruya, T., Urabe, M., Mizukami, H., Kume, A., Nakamura, M., et al. (2013). CD19 target-engineered T-cells accumulate at tumor lesions in human B-cell lymphoma xenograft mouse models. *Biochem. Biophys. Res. Commun.* 438, 84–89. <https://doi.org/10.1016/j.bbrc.2013.07.030>.
29. Kadoch, C., Dinca, E.B., Voicu, R., Chen, L., Nguyen, D., Parikh, S., Karrim, J., Shuman, M.A., Lowell, C.A., Treseler, P.A., et al. (2009). Pathologic correlates of primary central nervous system lymphoma defined in an orthotopic xenograft model. *Clin. Cancer Res.* 15, 1989–1997. <https://doi.org/10.1158/1078-0432.ccr-08-2054>.
30. Jahnke, K., Muldoon, L.L., Varallyay, C.G., Lewin, S.J., Brown, R.D., Kraemer, D.F., Soussain, C., and Neuwelt, E.A. (2009). Efficacy and MRI of rituximab and methotrexate treatment in a nude rat model of CNS lymphoma. *Neuro Oncol.* 11, 503–513. <https://doi.org/10.1215/15228517-2008-119>.
31. Muldoon, L.L., Lewin, S.J., Dósa, E., Kraemer, D.F., Pagel, M.A., Doolittle, N.D., and Neuwelt, E.A. (2011). Imaging and therapy with rituximab anti-CD20 immunotherapy in an animal model of central nervous system lymphoma. *Clin. Cancer Res.* 17, 2207–2215. <https://doi.org/10.1158/1078-0432.ccr-10-2923>.
32. Soussain, C., Muldoon, L.L., Varallyay, C., Jahnke, K., DePaula, L., and Neuwelt, E.A. (2007). Characterization and magnetic resonance imaging of a rat model of human B-cell central nervous system lymphoma. *Clin. Cancer Res.* 13, 2504–2511. <https://doi.org/10.1158/1078-0432.ccr-06-2379>.
33. Donnou, S., Galand, C., Daussy, C., Crozet, L., Fridman, W.H., Sautès-Fridman, C., and Fisson, S. (2011). Immune adaptive microenvironment profiles in intracerebral and intrasplenic lymphomas share common characteristics. *Clin. Exp. Immunol.* 165, 329–337. <https://doi.org/10.1111/j.1365-2249.2011.04416.x>.
34. Ben Abdelwahed, R., Donnou, S., Ouakrim, H., Crozet, L., Cosette, J., Jacquet, A., Tourais, I., Fournès, B., Gillard Bocquet, M., Miloudi, A., et al. (2013). Preclinical study of Ublituximab, a Glycoengineered anti-human CD20 antibody, in murine models of primary cerebral and intraocular B-cell lymphomas. *Invest. Ophthalmol. Vis. Sci.* 54, 3657–3665. <https://doi.org/10.1167/iov.12-10316>.
35. Montesinos-Rongen, M., Sánchez-Ruiz, M., Brunn, A., Hong, K., Bens, S., Perales, S.R., Cigudosa, J.C., Siebert, R., and Deckert, M. (2013). Mechanisms of intracerebral lymphoma growth delineated in a syngeneic mouse model of central nervous system lymphoma. *J. Neuropathol. Exp. Neurol.* 72, 325–336. <https://doi.org/10.1097/NEN.0b013e31828b7a98>.
36. Tateishi, K., Miyake, Y., Kawazu, M., Sasaki, N., Nakamura, T., Sasame, J., Yoshii, Y., Ueno, T., Miyake, A., Watanabe, J., et al. (2020). A Hyperactive RelA/p65-Hexokinase 2 Signaling Axis Drives Primary Central Nervous System Lymphoma. *Cancer Res.* 80, 5330–5343. <https://doi.org/10.1158/0008-5472.can-20-2425>.
37. Pouzoulet, F., Alentorn, A., Royer-Perron, L., Assayag, F., Mokhtari, K., Labiod, D., Le Garff-Tavernier, M., Daniau, M., Menet, E., Peyre, M., et al. (2019). Primary CNS lymphoma patient-derived orthotopic xenograft model capture the biological and molecular characteristics of the disease. *Blood Cells Mol. Dis.* 75, 1–10. <https://doi.org/10.1016/j.bcmd.2018.11.005>.
38. Etchin, J., Sanda, T., Mansour, M.R., Kentsis, A., Montero, J., Le, B.T., Christie, A.L., McCauley, D., Rodig, S.J., Kauffman, M., et al. (2013). KPT-330 inhibitor of CRM1 (XPO1)-mediated nuclear export has selective anti-leukaemic activity in preclinical models of T-cell acute lymphoblastic leukaemia and acute myeloid leukaemia. *Br. J. Haematol.* 161, 117–127. <https://doi.org/10.1111/bjh.12231>.
39. Tai, Y.T., Landesman, Y., Acharya, C., Calle, Y., Zhong, M.Y., Cea, M., Tannenbaum, D., Cagnetta, A., Reagan, M., Munshi, A.A., et al. (2014). CRM1 inhibition induces tumor cell cytotoxicity and impairs osteoclastogenesis in multiple myeloma: molecular mechanisms and therapeutic implications. *Leukemia* 28, 155–165. <https://doi.org/10.1038/leu.2013.115>.
40. Zhong, Y., El-Gamal, D., Dubovsky, J.A., Beckwith, K.A., Harrington, B.K., Williams, K.E., Goettl, V.M., Jha, S., Mo, X., Jones, J.A., et al. (2014). Selinexor suppresses downstream effectors of B-cell activation, proliferation and migration in chronic lymphocytic leukemia cells. *Leukemia* 28, 1158–1163. <https://doi.org/10.1038/leu.2014.9>.
41. Muqbil, I., Aboukameel, A., Elloul, S., Carlson, R., Senapedis, W., Baloglu, E., Kauffman, M., Shacham, S., Bhutani, D., Zonder, J., et al. (2016). Anti-tumor activity of selective inhibitor of nuclear export (SINE) compounds, is enhanced in non-Hodgkin lymphoma through combination with mTOR inhibitor and dexamethasone. *Cancer Lett.* 383, 309–317. <https://doi.org/10.1016/j.canlet.2016.09.016>.
42. Davis, R.E., Ngo, V.N., Lenz, G., Tolar, P., Young, R.M., Romesser, P.B., Kohlhammer, H., Lamy, L., Zhao, H., Yang, Y., et al. (2010). Chronic active B-cell-receptor signalling in diffuse large B-cell lymphoma. *Nature* 463, 88–92. <https://doi.org/10.1038/nature08638>.
43. Kaur, V., and Swami, A. (2017). Ibrutinib in CLL: a focus on adverse events, resistance, and novel approaches beyond ibrutinib. *Ann. Hematol.* 96, 1175–1184. <https://doi.org/10.1007/s00277-017-2973-2>.
44. Li, C.J., Jiang, C., Liu, Y., Bell, T., Ma, W., Ye, Y., Huang, S., Guo, H., Zhang, H., Wang, L., et al. (2019). Pleiotropic Action of Novel Bruton's Tyrosine Kinase Inhibitor BGB-3111 in Mantle Cell Lymphoma. *Mol. Cancer Ther.* 18, 267–277. <https://doi.org/10.1158/1535-7163.mct-18-0478>.

STAR★METHODS

KEY RESOURCES TABLE

REAGENT or RESOURCE	SOURCE	IDENTIFIER
<i>Antibodies</i>		
CD19	Biologend; Abcam	Cat # 302244; ab134114
CD20	Biologend; Abcam	Cat # 302326; ab64088
CD19 isotype antibodies	Biologend	Cat # 400161
CD20 isotype antibodies	Biologend	Cat # 400149
p-BTK	Abcam	ab68217
BTK	Abcam	ab208937
p-Erk1/2	Cell Signaling Technology	Cat # 4370
Erk1/2	Cell Signaling Technology	Cat # 4695
p-AKT	Cell Signaling Technology	Cat # 4060
AKT	Cell Signaling Technology	Cat # 4691
PAX5	Abcam	ab109443
GFAP	Santa Cruz	SC-33673
Ki-67	Cell Signaling Technology	Cat # 9449
CyclinB1	Cell Signaling Technology	Cat # 12231
CyclinA2	Abcam	ab181591
Cleaved PARP	Cell Signaling Technology	Cat # 5625
Cleaved caspase-3	Cell Signaling Technology	Cat # 9661
Bax	Cell Signaling Technology	Cat # 5023
β-actin	Cell Signaling Technology	Cat # 3700
Goat antimouse	ZSGB-BIO	ZB-2305
Goat antirabbit	ZSGB-BIO	ZB-2301
Alexa Fluor® 488 goat anti-Rabbit	ZSGB-BIO	ZB-0511
<i>Chemicals, peptides, and recombinant proteins</i>		
DMEM/F12	HyClone	SH30023.01
Neurobasal	Invitrogen	Cat # 21103049
N2	Invitrogen	Cat # 17502048
B27	Invitrogen	Cat # 17504044
2-mercaptoethanol	Invitrogen	Cat # 21985023
Insulin human recombinant	YESEN	Cat # 40112ES25
Glutamax	Life Technologies	Cat # 35050-061
Sodium pyruvate	Life Technologies	Cat # 11360-070
MEM-non-essential amino acids	Sigma	M7145
EGF	Peptotech	AF-100-15
bFGF	Peptotech	100-18B
Matrigel	Corning	Cat # 356234
Penicillin-streptomycin	Biosharp	BL505A
Selinexor	Meilun Biotechnology Co., Ltd.	MB4546
Zanubrutinib	BeiGene Co., Ltd.	Gift
MK-2206 (AKT inhibitor)	Selleck	S1078
SC79 (AKT activator),	Selleck	S7863

(Continued on next page)

Continued

REAGENT or RESOURCE	SOURCE	IDENTIFIER
SCH772984 (ERK inhibitor)	Selleck	S7101
Human Trustain FcX™	BioLegend	Cat # 422302
DAPI	Solarbio	C0065
Counting Kit 8	DOJINDO	CK04
TRlzol reagent	Thermo Fishe	Cat # 15596026
RIPA buffer	Solarbio	R0010
Protease inhibitor	Bimake	B4001
Phosphatase inhibitor	Solarbio	P1260
5 × loading buffer	Solarbio	P1040
SDS-polyacrylamide gel electrophoresis	Epizyme	PG112
DAB	ZSGB-BIO	ZLI-9017
Hematoxylin	ZSGB-BIO	ZLI-9610

Critical commercial assays

TUNEL detection kit	Beyotime	C1088
BCA Protein Assay Kit	Solarbio	PC0020
Annexin V FITC Apop Dtec Kit I	BD	Cat # 556547
Cell cycle and apoptosis analysis kit	Beyotime	C1052

Deposited data

RNA-seq	This paper	CNGB: CNP0005523 https://db.cngb.org/mycngbdb/submissions/project
---------	------------	--

Experimental models: Cell lines

PCNSL cells (male)	This paper	N/A
--------------------	------------	-----

Experimental models: Organisms/strains

NOD-Prkdcscid IL2rgnull mice (female)	SPF (Beijing) Bioscience Co., Ltd.	NTG mice
---------------------------------------	------------------------------------	----------

Software and algorithms

CompuSyn software (version 1)	Dorothy Chou	https://www.combosyn.com/
R (version 4.3.1)	R Development Core Team	https://www.r-project.org/
GraphPad Prism (version 9.5.1)	GraphPad Software	https://www.graphpad.com/features
Flowjo software (version 10.8.1)	BD	https://www.flowjo.com/
ImageJ software	NIH	https://hpc.nih.gov/apps/Fiji.html

RESOURCE AVAILABILITY

Lead contact

Further information and requests for resources and reagents should be directed to and will be fulfilled by the lead contact, Dr. Wenbin Li (liwenbin@ccmu.edu.cn).

Materials availability

The PCNSL primary cells in this paper are available upon request from the corresponding author.

Data and code availability

- RNA-seq data have been deposited at China National GeneBank (CNGB) and are publicly available as of the date of publication. Accession numbers are listed in the [key resources table](#). Original western blot images are available in the [supplemental information](#).
- This paper does not report any original code.
- Any additional information required to reanalyze the data reported in this paper is available from the [lead contact](#) upon request.

EXPERIMENTAL MODEL AND STUDY PARTICIPANT DETAILS

Primary cells

Primary cells (male) were established based on biopsy tissue of PCNSL patients. Human tumor biopsy tissues were obtained from three male patients (yellow race, China) diagnosed with PCNSL at the Beijing Tiantan Hospital, Capital Medical University. The patient provided written informed consent for studies of their tumor and the protocol was approved by the institutional review board and the research ethics committee of Beijing Tiantan Hospital, Capital Medical University. Primary cells were cultured in a humidified incubator at 37°C and 5% CO₂/95% air (v/v).

Animal

All animal experiments were conducted at the Beijing Institute of Neurosurgery. All experimental protocols for the procedures with animals were approved by the animal ethics committee of Beijing Tiantan Hospital, Capital Medical University (approval number 202101024). 6–8 weeks female NTG mice (NOD-Prkdcscid IL2rgnull) weighing approximately 18–20 g of were purchased from the SPF (Beijing) Bioscience Co., Ltd. and maintained in an SPF animal housing facility. Mice had access to food and water *ad libitum* and were kept at a constant temperature on a 12-h light/dark cycle.

METHOD DETAILS

Establishment of PCNSL primary cells

Human tumor biopsy tissues were obtained from three patients diagnosed with PCNSL at the Beijing Tiantan Hospital, Capital Medical University. All three patients were immunocompetent and free of EBV infection. To efficiently use limited PCNSL biopsy tissue, we manufactured “dimpled” parafilm by homemade combination tools (composed of 10 mL centrifuge tube and 200 μ L PCR tube), yielding reproducibly sized dimpled indentations or molds (Figure S1A). The PCNSL biopsy sample was dissected to 1 mm³–2 mm³ tissue blocks with sterile scissors and then added at a volume ratio of 1:4 of PCNSL-specific culture medium and Matrigel (Corning #356234). Tissue blocks of 1 mm³–2 mm³ were mixed with matrigel and 20 μ L suspension was rapidly added to each mold (Figure S1B). The mixture was allowed to solidify in a CO₂ incubator before being transferred to a PCNSL-specific culture medium. After observing the formation of cell clusters, the cells were passaged. All processes were performed in a biosafety cabinet and required sterile operations.

The detailed steps were as follows: (1) Use parafilm to create 12–16 concave micro-wells on a 10 μ L pipette tip box plate. (2) The fresh PCNSL biopsy sample was placed in DMEM/F12 cultured medium and cut into 1 mm³–2 mm³ tissue blocks with sterile scissors. (3) Centrifuge the DMEM/F12 medium containing 1 mm³–2 mm³ tissue blocks, and then discard the culture medium. (4) Add PCNSL-specific culture medium and matrigel in a ratio of 1:4, thoroughly mix them. And add 20 μ L of the mixture to each concave micro-well. (5) Place the parafilm on a culture dish and add 1–2 mL of PBS (Figure S1B). Then, place it in a 37°C, 5% CO₂ incubator and wait for 1 h for the matrigel to solidify. (6) The solidified matrigel containing PCNSL tissue was completely removed and placed in PCNSL-specific culture medium for cultivation. (7) The culture medium was changed every 3 to 4 days until the formation of PCNSL cell clusters.

The PCNSL-specific culture medium effectively simulated the CNS microenvironment in which PCNSL survived. The culture medium contained a 1:1 mixture of DMEM/F12 (HyClone, SH30023.01) and Neurobasal (Invitrogen, #21103049) contained 1:200 N2 supplement (Invitrogen, #17502048), 1:100 B27 supplement (Invitrogen, #17504044), 3.5 μ L/L 2-mercaptoethanol (Invitrogen, #21985023), 2.5 μ g/mL insulin human recombinant (YESEN, #40112ES25), 1:100 glutamax (Life Technologies, #35050–061), 1:100 sodium pyruvate (Life Technologies, #11360–070), 1:200 MEM-non-essential amino acids (Sigma, M7145), 20 ng/mL EGF (Peprotech, AF-100-15), 20 ng/mL bFGF (Peprotech, 100-18B), and 1:100 penicillin-streptomycin (Biosharp, BL505A).

Drugs and reagents

Zanubrutinib was gifted by BeiGene Co., Ltd. (Beijing, China), and Selinexor was purchased from Meilun Biotechnology Co., Ltd. (Dalian, China). MK-2206 (an AKT inhibitor), SC79 (an AKT activator), and SCH772984 (an ERK inhibitor) were purchased from Selleck (USA). It was initially dissolved in 100% DMSO (Sigma-Aldrich, Germany) and stored at –20°C. The control for oral selinexor was 0.6% plasdone PVP K-30 (Solarbio, P8060). Methylcellulose (0.5% methylcellulose; BioTopped, M6080) was used as the control for oral zanubrutinib.

Flow cytometry

Primary PCNSL cells were collected and fixed in cold 2% paraformaldehyde for 15 min. The cells were then washed thrice with cold PBS. For CD19 and CD20 expression analysis, cells were blocked in Human Trustain FcX (BioLegend, #422302) at 37°C for 30 min and divided into blank, isotype, and detection tubes. Cells in the isotype tube were incubated with CD19 (Biolegend, #400161) and CD20 isotype antibodies (Biolegend, #400149), followed by incubation with anti-human CD19 (Biolegend, #302244) and anti-human CD20 (Biolegend, #302326) antibodies at room temperature for 30 min. Finally, cells were washed twice and resuspended in cold PBS. All the analyses were performed using Flowjo software (version 10.8.1, BD).

Immunofluorescence

PCNSL primary cells grown on glass coverslips pretreated with TC (Solarbio, YA0350) and fixed for 15 min in 2% paraformaldehyde at room temperature, and then incubated with 5% BSA at room temperature for 1 h before incubation with anti-CD20 antibody (Abcam, ab64088) and anti-CD19 antibody (Abcam, ab134114) overnight at 4°C. Cells were washed thrice in PBS for 5 min each, and then incubated with Alexa Fluor 488 goat anti-Rabbit IgG (H + L) (ZSGB-BIO, ZF-0511) secondary antibodies at room temperature for 1 h. After a final wash with PBS, cells were incubated with DAPI (Solarbio, C0065) for 5 min. The images were captured using an Evos FL Auto 2 fluorescence microscope (Thermo Fisher Scientific).

Cell proliferation assay

For half-maximal inhibitory concentration (IC50) of drug, PCNSL Cells were seeded in 96-well plate at a density of 8000 cells per 100 μ L and treated with different concentrations of selinexor and zanubrutinib for 48 h. For time-course analysis, PCNSL cells were exposed to fixed concentrations of selinexor and different concentrations of zanubrutinib for 24 h, 48 h and 72 h. Cells were treated with selinexor, zanubrutinib, MK-2206 (AKT inhibitor), SC79 (AKT activator), and SCH772984 (ERK inhibitor) for 24 h for the cell proliferation assay. The Cell Counting Kit 8 (DOJINDO, CK04) assay was performed to evaluate cell proliferation. The absorbance was measured using a spectrophotometer (TECAN SPARK 10 M, Switzerland). The experiments were repeated in biological triplicates.

Apoptotic analysis, cell-cycle assays, and TUNEL assay

Cells were treated with a fixed concentration of selinexor alone or in combination with different concentrations of zanubrutinib for 24 h for apoptosis and cell cycle analysis. According to the protocol, performed apoptosis analysis using the Annexin V FITC Apop Dtec Kit I (BD, #556547). For cell cycle assays, cells were stained using the cell cycle and apoptosis analysis kit (Beyotime, C1052) according to the manufacturer's protocol. Finally, the cells were analyzed using a flow cytometer (Beckman CytoFLEX, USA). TUNEL is a method for detecting DNA fragmentation by labeling the 3'-hydroxyl termini in the double-strand DNA breaks generated during apoptosis. Orthotopic PCNSL xenograft mice models were treated with selinexor and zanubrutinib alone or in combination, and brain tissue were fixed in 4% paraformaldehyde, embedded in paraffin and cut into 5 μ m sections. A TUNEL assay was then conducted to examine DNA fragmentation using the detection kit (Beyotime, C1088) according to the manufacturer's instructions. Images were captured by Zeiss LSM 710 confocal microscope (Zeiss, Germany). The experiments were repeated in biological triplicates.

RNA sequencing and analysis

Cells were treated with selinexor 0.05 μ M and zanubrutinib 5 μ M alone or in combination for 24 h. The experiments were repeated in biological triplicates. The collected cells were lysed using TRIzol reagent (Thermo Fisher, #15596026). Total RNA was extracted and reverse transcribed into cDNA, and RNA quantification and qualification, library preparation, clustering and sequencing, read mapping, and data processing were performed by Novogene Bioscience (Beijing, China). Differential expression analysis was performed using the DESeq2 R package (1.40.1), and genes with $|\log_2$ fold change $> \log_2$ (1.5) and adjusted $p < 0.05$ were defined as differential genes. Kyoto Encyclopedia of Genes and Genomes (KEGG) pathway enrichment analyses were performed using the clusterProfiler R package (v4.8.1). A heatmap of the target gene was generated and visualized using the pheatmap R package (1.0.12).

Western blotting

Cells were treated with selinexor, zanubrutinib, MK-2206 (AKT inhibitor), or SC79 (AKT activator), alone or in combination, for 24 h. Collected cultured cells were lysed on ice for 30 min in RIPA buffer (Solarbio, R0010) mixed with protease inhibitor (Bimake, #B4001) and phosphatase inhibitor (Solarbio, P1260). After centrifugation at 12,000 \times g for 10 min, the supernatant was placed in a new EP tube. The protein quantification was performed using BCA Protein Assay Kit (Solarbio, PC0020) according to protocol. Then 5 \times loading buffer (Solarbio, P1040) was added based on the quantification results, and the samples were boiled at 95°C for 10 min. After the samples were cooled to room temperature, proteins were separated by SDS-polyacrylamide gel electrophoresis (Epizyme, PG112) and transferred to an NC membrane (PALL, #66485). The primary antibodies used in this study included antibodies against Phospho-BTK (p-BTK) (Abcam, ab68217, 1:1000), BTK (Abcam, ab208937, 1:1000), Phospho-p44/42 MAPK (p-Erk1/2) (Cell Signaling Technology, #4370, 1:1000), p44/42 MAPK (Erk1/2) (Cell Signaling Technology, #4695, 1:1000), Phospho-AKT (p-AKT) (Cell Signaling Technology, #4060, 1:1000), AKT (Cell Signaling Technology, #4691, 1:1000), CyclinB1 (Cell Signaling Technology, #12231, 1:1000), CyclinA2 (Abcam, ab181591, 1:2000), Cleaved PARP (Cell Signaling Technology, #5625, 1:1000), Cleaved caspase-3 (Cell Signaling Technology, #9661, 1:1000), Bax (Cell Signaling Technology, #5023, 1:1000), β -actin (Cell Signaling Technology, #3700, 1:1000). The secondary antibodies were goat antimouse IgG antibody (ZSGB-BIO, ZB-2305, 1:3000), goat anti-rabbit IgG antibody (ZSGB-BIO, ZB-2301, 1:3000). The results were analyzed using chemiluminescence detection system (Gene, China). The experiments were repeated in biological triplicates.

Hematoxylin-eosin (HE) and immunohistochemical (IHC) staining

The tumor sample and brain tissue sample from experimental mice were preserved in 4% paraformaldehyde and embedded in paraffin. For HE staining, the brain slides were incubated with hematoxylin and eosin. For IHC staining, antigen retrieval was performed by application of citrate buffer pH 6.00 for 15 min. The slides were incubated with primary antibody against CD20 (Abcam, ab64088, 1:100), CD19 (Abcam,

ab134114, 1:500), PAX5 (Abcam, ab109443, 1:1000), GFAP (Santa Cruz, SC-33673, 1:100) and Ki 67 (Cell Signaling Technology, #9449, 1:800) overnight at 4°C and then with HRP-conjugated secondary antibody (ZSGB-BIO, ZB-2305/ZB-2301, 1:500) at room temperature for 1 h, followed by staining with DAB (ZSGB-BIO, ZLI-9017) for 15 min, washed with PBS, stained with hematoxylin (ZSGB-BIO, ZLI-9610). Images were captured with Zeiss Axio Vert.A1 reversed microscope (Zeiss, Germany).

Subcutaneous and orthotopic PCNSL xenograft mice models

Six to eight-week-old female NTG mice (NOD-Prkdcscid IL2rgnull) were used to develop subcutaneous and orthotopic xenograft models of PCNSL. NTG mice were obtained from SPF (Beijing) Bioscience Co., Ltd. (Beijing, China). For the subcutaneous model, primary PCNSL cells (1×10^7) in PCNSL-specific culture medium with Matrigel (1:1 ratio) were injected subcutaneously into the left dorsal region of the mice. After 28 days, the xenografts were removed for immunohistochemical staining.

In the orthotopic xenograft model, primary PCNSL cells were stably transfected with luciferase. Lentivirus containing luciferase gene, green fluorescent protein gene, and anti-puromycin gene (LV-Luc2-ZsGreen-Puro-CON) was added to the PCNSL-specific medium with 3×10^5 primary cells and incubated (at 37°C, 5% CO₂) for 6 h. The final titer of the lentivirus was 3×10^7 transduction units/mL (Tu/mL). The cells were then centrifuged, resuspended, and transferred to a fresh PCNSL-specific culture medium. After 72 h of transfection, the transfection efficiency of the PCNSL cells was confirmed by observing green fluorescent proteins using a fluorescence microscope. Subsequently, 0.2 µg/mL puromycin was added to the culture medium for selection. Further, 1×10^5 cells in 5 µL PBS were injected intracerebrally (coordinates: 1 mm posterior, 1.8 mm lateral right to the bregma, and 3.0 mm deep from the dura) with a Hamilton syringe at a rate of 1 µL/min using a brain stereotaxic injection apparatus (RWD, China). Tumor formation was monitored by bioluminescence imaging (BLI) using an IVIS Spectrum system (PerkinElmer, USA) on day 7 after intracerebral injection. For tumor formation, mice were randomly assigned to four groups (control, selinexor-, zanubrutinib-, and both selinexor and Zanubrutinib-treated). Selinexor (5 mg/kg, dissolved in 0.6% plasdone PVP K-29/32) and zanubrutinib (15 mg/kg, dissolved in 0.5% methylcellulose) was administered twice a week for three weeks. To monitor tumor growth in PCNSL xenografted mice, mice were injected intraperitoneally with 10 µL/g of 15 mg/mL D-luciferin potassium salt solution (PerkinElmer, #122799). Tumor size was analyzed and quantified using Living Image 4.4 software (PerkinElmer) and the total photons per second (ph/s) were recorded.

QUANTIFICATION AND STATISTICAL ANALYSIS

Statistical analysis

Values are expressed as mean \pm SD. The data were analyzed for statistical significance using the unpaired Student's t test and two-way ANOVA using GraphPad Prism 9 software for Windows. For two-group comparison, p values <0.05 was considered statistically significant. For omics analysis, values of False Discovery Rate (FDR) < 0.05 were accepted as statistically significant. The combination index (CI) for drug combinations was determined according to the Chou-Talalay method using CompuSyn software (version 1, Biosoft, UK). Combination index (CI) values of <1 , $= 1$, and >1 indicated synergistic, additive, and antagonistic effects, respectively. Survival analysis was performed using the Kaplan–Meier method. The protein, Ki 67 positive cells and TUNEL positive cells were quantified and analyzed using ImageJ software. Throughout the text, * $p < 0.05$, ** $p < 0.01$, *** $p < 0.001$, **** $p < 0.0001$; # $p < 0.05$, ## $p < 0.01$, ### $p < 0.001$, #### $p < 0.0001$. And comparisons were specifically indicated in the figure legends.